Nanoscale Advances

ROYAL SOCIETY OF CHEMISTRY

PAPER

View Article Online
View Journal | View Issue

Cite this: *Nanoscale Adv.*, 2026, **8**, 1888

Anti-inflammatory effects of curcumin carbon dots in an animal model of demyelination induced by lysolecithin

Ladan DaeiRezaei, [ac] Elham Parandavar, [bc] Mohammad Javan *[bc] and Maryam Nikkhah *[a]

Multiple Sclerosis (MS) is an autoimmune neurodegenerative disease that affects the central nervous system (CNS) characterized by myelin loss and axonal degeneration. Studies have shown that chronic inflammation followed by demyelination contributes to extensive myelin degradation. Thus far, despite disease-modifying treatments (DMTs) that delay disease progression, a definitive cure remains in demand due to the disease's uncertain etiology. Recent studies highlight carbon-based nanomaterials, particularly carbon dots (CDs), as promising drug carriers due to their antioxidant and anti-inflammatory effects, hydrophilicity, biocompatibility and fluorescence properties. In this study, curcumin-derived carbon dots (CurP-CDs) were synthesized *via* a one-pot hydrothermal method, and their physicochemical properties, *in vitro* antioxidant effects, and *in vivo* anti-inflammatory and neuroprotective effects were evaluated in C57BL/6 male mice subjected to demyelination through local lysolecithin injection. Histological analyses showed reduced myelin loss and preserved myelin basic protein levels in animals treated with CurP-CDs compared to controls at 3 and 7 days post-lysolecithin injection. In addition, immunostaining revealed decreased astrocyte and microglia activation, the leading cells in neuroinflammation and gliosis, indicating reduced inflammation.

Received 19th March 2025
Accepted 22nd December 2025

DOI: 10.1039/d5na00261c

rsc.li/nanoscale-advances

1 Introduction

Multiple Sclerosis (MS) is a chronic autoimmune disorder of the central nervous system (CNS) characterized by demyelination, plaque formation, axonal loss, and neurodegeneration. While the exact etiology remains unclear, it likely involves a combination of genetic and environmental factors.[1–3] Inflammatory responses, gliosis, oxidative stress, and mitochondrial dysfunction further drive tissue damage. Microglia at demyelination sites exhibit high NADPH oxidase activity, indicative of tissue oxidative damage.[4,5] T lymphocytes targeting myelin proteins such as Myelin Basic Protein (MBP), Proteolipid Protein (PLP), and Myelin Oligodendrocyte Glycoprotein (MOG) increase CNS infiltration of autoreactive immune cells. Imbalances between effector T cells and regulatory T cells, along with contributions from B cells and CNS-resident microglia and macrophages, exacerbate inflammation.[6,7] Following demyelination and inflammation, astrocytes and microglia form a dense mechano-chemical glial barrier that isolates lesions, restores the blood–brain barrier, and limits inflammation by reducing infiltration of inflammatory factors.[8] These lesions, or sclerosis, disrupt axonal conduction, affecting areas such as the optic nerves, ventricles, corpus callosum, brainstem, cerebellum, and spinal cord, leading to progressive tissue damage and atrophy.[9,10] The corpus callosum is notably vulnerable to early demyelination caused by lysophosphatyl choline (LPC) and is considered a hallmark structure affected in MS, making it a rational target for localized modeling of demyelination.[11]

To date, a variety of therapeutic approaches have been proposed for MS, such as anti-inflammatory strategies, mitochondrial protection, targeting of glial cells and lymphocytes, and the use of remyelinating agents. Despite available disease-modifying treatments, MS remains incurable, with current therapies mainly for relapse remitting multiple sclerosis (RRMS), focused on immunosuppression to prevent relapses. However, their systemic toxicity and poor CNS penetration highlight the urgent need for safe, effective agents with CNS bioavailability.[3,12]

Over the past two decades, research has highlighted nanomaterials as promising platforms for delivering therapeutics, immunomodulatory agents, and antigens. Their unique properties, such as improving drug solubility, facilitating targeted delivery, minimizing side effects, and enabling controlled release, make them highly effective in enhancing treatment outcomes.[6] Recent advancements in nanomaterials highlight

[a]*Department of Nanobiotechnology, Faculty of Biological Sciences, Tarbiat Modares University, Tehran, Iran. E-mail: m_nikkhah@modares.ac.ir*

[b]*Department of Physiology, Faculty of Medical Sciences, Tarbiat Modares University, Tehran, Iran. E-mail: mjavan@modares.ac.ir*

[c]*Institute for Brain and Cognition, Faculty of Medical Sciences, Tarbiat Modares University, Tehran, Iran*

their potential in both diagnosing and treating multiple sclerosis. These materials enhance drug delivery, provide neuroprotection, support cellular repair, and improve bio-sensing and bio-imaging, holding great potential for improving MS treatment and management approaches.[12–16]

Carbon dots (CDs), due to their biocompatibility, biodegradability, unique optical properties, extended π–π conjugation along with abundant functional groups (*e.g.*, amine and carboxyl) and the possibility to cross the blood–brain barrier[27–31] have gained great attention for the treatment of CNS disorders.[17–19] Studies have demonstrated that CDs from different sources have antioxidant and anti-inflammatory properties in chronic disease models involving inflammation, which is a key factor in MS pathology, highlighting their potential as promising candidates for new drug development.[18,20]

Prior studies have reported the anti-inflammatory properties of CDs synthesized from aspirin,[21] carbonized human hair,[22] genistein,[23] laccaic acid,[24] and ibuprofen.[25] Although remarkable progress has been made in targeting carbon dots to the CNS, most studies have focused on Alzheimer's and Parkinson's diseases, both of which are driven by protein aggregation and misfolding and do not reflect the autoimmune inflammatory nature of MS.[26] A study by J. Tosic *et al.* serves as one of the few examples in which the intraperitoneal injection of graphene quantum dots to an experimental autoimmune encephalomyelitis (EAE) model led to their accumulation in lymph nodes and the CNS. This treatment significantly reduced clinical symptoms, immune cell infiltration, demyelination, axonal damage, and apoptosis, while decreasing Th1 cells expressing interferon-γ, Th1-related transcription factor T-bet, and pro-inflammatory cytokines (TNF, IL-1, and GM-CSF), ultimately protecting oligodendrocytes and neurons from T-cell-induced damage *in vitro*.[27]

Furthermore, the precursor used in carbon dot (CD) synthesis significantly affects the biological functionality of the final product. Among various options, organic compounds with antioxidant and anti-inflammatory properties show promise for protecting the myelin sheath and offering neuroprotection.[28] Polyphenolic compounds, such as curcumin from turmeric, demonstrate strong antioxidant and anti-inflammatory properties.[29] Nonetheless, poor water solubility, low bioavailability and cellular uptake, and instability at physiological pH caused by rapid autoxidation limit its use.[29] Several strategies such as conjugation/encapsulation have been reported to overcome curcumin poor solubility and stability under physiological conditions. For instance, conjugated linoleic acid-curcumin was shown to reduce oxidative stress, spatial memory issues, and memory impairment in an ethidium bromide model of demyelination.[30] Moreover, the anti-inflammatory and antioxidant effects of polymerized nano-curcumin were confirmed in the EAE mouse model.[31] Also, dendrosomal nano-curcumin effects on oligodendrogenesis and remyelination were proved *in vitro* and in the EAE mouse model. Nano-curcumin protected oligodendrocyte cell lines, reduced myelin loss, and decreased astrocyte and microglia counts, alleviating microgliosis and astrogliosis in the cuprizone demyelination model.[32,33] Besides, Fe_3O_4@carbon dots enhanced curcumin delivery, reduced Aβ-induced toxicity and ROS production, and supported neuronal protection.[34] Converting curcumin into carbon dots is another strategy to address curcumin limitations such as poor solubility and low bioavailability.[35] It was shown that Cur-CDs possess intrinsic antioxidant, anti-inflammatory, and neuroprotective properties, along with excellent water solubility, photostability, and biocompatibility. Therefore, in this study, carbon dots were synthesized *via* a one-pot hydrothermal method using curcumin, phenylalanine, citric acid, and urea. Curcumin was used in the highest molar ratio owing to its potent antioxidant and anti-inflammatory properties, while the other precursors were chosen to improve biocompatibility and incorporate functional groups. The resulting CDs were evaluated for their effects on demyelination and inflammation in a lysolecithin-induced animal model.

2 Methods and materials

2.1. Curcumin carbon dot synthesis and characterization

Carbon dots were synthesized through a one-pot hydrothermal method. Briefly, 200 mM curcumin (Biobasic; CAS#: 458-37-7), 100 mM L-phenylalanine (Biobasic; CAS#: 63-91-2), 170 mM citric acid (Merck; CAS#: 73-22-3), and 80 mM urea were dissolved in 15 ml deionized water (Sabalan Nanochemistry; CAS#:7732-18-5) and heated in a Teflon container inside an autoclave in an oven (Jeio Tech Vacuum Oven) at 200 °C for 4 hours, resulting in a dark brown carbonized material, which was ground into a brown powder. Thereafter, 300 mg of the powder was dispersed in 1 ml phosphate-buffered saline and sonicated (POWERSONIC 405) for 30 minutes at RT, followed by centrifugation at 4000 rpm for 15 minutes (WiseSpin Centrifuge) to remove large aggregates. The supernatant was filtered using a PTFE syringe filter (0.22 μm, Jet Biofil), and the filtrate was dialysed against phosphate buffered saline (PBS) for 24 hours using 0.1–0.5 kDa CE dialysis tubing (Spectrum Laboratories). The dialysed CurP-CDs were dried and weighted.

The optical properties of the synthesized carbon dots were determined using ultraviolet-visible (UV-vis) spectroscopy (Peybord Dualbin) and fluorescence spectrometry (Perkin Enspire). Functional groups present in the carbon dots were identified through Fourier-transform infrared spectroscopy (FTIR) (Frontier-PerkinElmer instrument). Images were obtained using a transmission electron microscope, Titan G2 60–300 (FEI), at an accelerating voltage of 300 kV. Images were captured using a BM UltraScan CCD camera (Gatan) and were analyzed by Image J software to obtain the average size of CDs. The surface morphology and roughness of the microspheres were characterized using an atomic force microscope (AFM, Brisk, Iran). The zeta potential was determined using a dynamic light scattering (DLS) instrument from the Zetasizer Nano ZS series (Malvern, UK).

2.2. Evaluation of antioxidant capacities of CurP-CDs

The antioxidant activity of CurP-CDs was evaluated using the DPPH colorimetric assay. DPPH, a stable free radical, is purple

in its oxidized form and turns yellow when reduced by antioxidants. In the assay, 180 μl of 0.1 mM DPPH (Molekula; CAS#:1898-66-4) solution in ethanol (Merck; CAS#:64-17-5) was added to a 96-well plate, followed by the addition of 20 μl of CurP-CD solutions at varying concentrations (15, 30, 150, 300, 600, and 1000 μg ml^{-1}). Distilled water was used as the negative control, while ascorbic acid at a concentration of 2 mg ml^{-1} served as the positive control. After 30 minutes incubation at RT, the absorbance of the wells was read at 517 nm (Citation TM 3-Imaging reader, BioTeck).

The antioxidant activity was calculated using the following formula:

$$\mathrm{RSA}\% = [(A_b - A_s)/A_b] \times 100 \quad (1)$$

where A_b represents the mean absorbance of the negative control used as the blank, and A_s denotes the mean absorbance of the sample.[36]

2.3. Evaluation of CurP-CD cytotoxicity

To assess nanoparticle cytotoxicity, U-87 MG cells (purchased from the Royan Institute of Iran) were seeded (8000 cells per well) in a 96-well plate using DMEM-F12 (Gibco) containing 10% FBS (Gibco) and 1% penstrep (Sigma-Aldrich) and treated with CurP-CDs (0–300 μg ml^{-1}) for 24 hours. Subsequently, cells were washed 3 times with PBS, MTT reagent was added, and the plate was incubated (37 °C, 5% CO_2) for 4 hours. After dissolving formazan crystals in DMSO, the absorbance (570 nm) was measured.

Viability (%) was calculated as:

$$\text{Cell viability } \% = (A_t/A_c) \times 100 \quad (2)$$

where A_t and A_c are the mean absorbance of the treated samples and control, respectively.

2.4. *In vivo* studies

2.4.1. Animals. Male C57BL/6 mice (8–10 weeks old, 20–25 g) were obtained from the Pasteur Institute, Karaj, Iran, and housed under standard conditions: 12 h light/dark cycles, controlled temperature (25 ± 2 °C), free access to food and water, and 5 mice per cage. After one week of acclimatization, surgical procedures were conducted. All animal care protocols and experiments adhered to international ethical guidelines for laboratory animals and were approved by the Tarbiat Modares University Ethics Committee (Ethics Code: IR.MODARES.AEC.1402.004).

2.4.2. Induction of demyelination by lysolecytin (LPC). Lysolecithin, or lysophosphatidylcholine (LPC), disrupts myelin sheaths, induces oligodendrocyte death, and activates T and B cells, macrophages, and microglia; therefore, it triggers inflammation that peaks within 2–3 days after LPC administration. Myelin damage peaks at 7 days, with remyelination resuming *via* oligodendrocyte progenitor migration and maturation by day 14, providing a suitable model to study a cycle of MS remission and relapse.[9,37] In this study, 1 μL of 1% LPC solution (Sigma-Aldrich, CAS# 9008-30-4) was injected at 0.7 mm mediolateral and 1.06 mm posterior to the bregma, and 2 mm below the dura, into the right hemisphere corpus callosum using a Hamilton syringe. Immediately following LPC injection, 2 μl of CurP-CDs (1 mg ml^{-1}) was administered bilaterally to ventricles at 1 mm mediolateral, 0.58 mm posterior to the bregma and 2 mm below the dura. As the control for CurP-CDs treatment, 2 μl of PBS was injected at the same coordinates in LPC treated animals (Table 1). Solutions were injected over 5 minutes, after which the needle remained in place for an additional 5 minutes to prevent solution reflux before being gently withdrawn. The skin was sutured, and mice were placed on a heating pad until recovery from anesthesia.

Table 1 Coordinates of injections relative to the bregma

	Anterio-posterior	Mediolateral	Dorsoventral
LPC	−1.06 mm	−0.7 mm	−2 mm
CDs	−0.58 mm	−1 mm	−2 mm
PBS	−0.58 mm	−1 mm	−2 mm

2.4.3. Experiment design for treatment study. Animals were divided into 5 groups each including 5 mice. The interventions and treatments in different groups as well as the time of sacrificing of mice are mentioned in Table 2. To evaluate gliosis, brain samples harvested on days 3 and 7 post injection were subjected to immuno-histofluorescent staining with GFAP and Iba-1 markers. To evaluate myelin content in brain tissues, samples harvested at the same time points were examined using luxol fast blue (LFB), FluoroMyelin, and MBP staining.

2.4.4. Tissue preparation. Intraperitoneal injection of 10% chloral hydrate (Merck, CAS# 302-17-0) (50 mg kg^{-1}) deeply anesthetized animals for transcardial perfusion using 0.1 M PBS, followed by paraformaldehyde 4% (Daejung Chemicals CAS# 30525-89-4). Brains were post-fixed in PFA 4% for 12–16 hours, dehydrated in 30% sucrose for 24 hours, and embedded in optimum cutting temperature medium (OCT, Bio-optica). Coronal sections (8 μm) were prepared using cryostat (Histo-Line Laboratories) and stored at −20 °C until staining.

2.4.5. FluoroMyelin staining. Slides were left at room temperature for 30 minutes before staining, followed by PBS washing (5 min, three times) to washout OCT. FluoroMyelin (FM), a myelin-specific fluorescent dye (1:300, ThermoFisher,

Table 2 The animal groups and the sampling time, including the intact group, which consisted of non-LPC and untreated mice; the model group, which showed the manifestations of the disease; and finally the treated group, which received carbon dots immediately after receiving lysolecitin

Groups	*n*	Treatments
Intact	5	No interventions
Model 3 dpi	5	LPC + PBS
Model 7 dpi	5	LPC + PBS
Treated 3 dpi	5	LPC + CurP-CDs
Treated 7 dpi	5	LPC + CurP-CDs

dpi denotes days post injection.

Cat#F34652), was used to assess the effects of CDs on myelin content and to ensure that the demyelination model was appropriately induced. Slides were washed three times with PBS, incubated with the dye for 30 minutes at room temperature, and washed an additional three times. Image J software was used to quantify fluorescence microscopy images.

The fluorescence intensity of the corpus callosum was corrected for background signal. Three slides per animal were analyzed, and the corrected values were averaged. These averages were then normalized to the mean fluorescence intensity of the myelinated region in the intact group, with the results expressed as percentages.

2.4.6. Luxol fast blue staining. LFB, a lipophilic dye, was used to assess demyelinated areas. Slides were washed thrice with PBS, placed in graded ethanol (100% and 95%, 5 min each), immersed in 0.1% LFB (Solvent Blue 38, Sigma-Aldrich, CAS#1328-51-4) for 1 hour at 60 °C, and excess dye was removed with 95% ethanol and distilled water. Sections were counterstained in 0.05% lithium carbonate (Sigma-Aldrich, CAS#554-13-2) (30 s) and washed with distilled water. Cresyl violet (Merck, Cat#K2247947) (1 min) was used to stain nuclei, then sections were dehydrated using ethanol (95% & 100%, 5 minute each), cleared in xylene, and mounted with coverslips using Entellan. To quantify Luxol fast blue staining data, the myelinated area was measured in ImageJ using a defined threshold. Three slides per animal were analyzed, and the values were averaged. These averages were then normalized to the mean myelinated area of the intact group.

2.4.7. Immunostaining. Immunofluorescent staining for myelin protein MBP, astrocyte marker GFAP, and microglia marker Iba-1 were performed as follows: cryosections were incubated at room temperature for 30 minutes, washed three times with PBS (5 minutes each), and antigen retrieval was carried out using citrate buffer for 30 minutes. Sections were permeabilized with 0.3% Triton X-100 (Sigma-Aldrich, CAS# 9036-19-5) for one hour, then blocked with blocking solution of 10% normal goat serum (NGS) and 0.2% Triton X-100 in PBS for one hour. Primary antibodies were applied overnight at 4 °C, followed by PBS washes and secondary antibody incubation for two hours at room temperature. Antibodies were diluted in blocking solution. Nuclear staining was performed with DAPI (Sigma-Aldrich; Cat#D-9542) for 5–10 minutes. Slides were analyzed with a fluorescence microscope, and signal intensity for MBP was quantified using ImageJ, while Iba-1+ and GFAP+ cell counts were expressed as a percentage of total nuclei. Primary antibodies included chicken polyclonal anti-MBP (1:1000, Aves Labs Cat#MBP-0020), rabbit polyclonal anti-GFAP (1:500, Dako, Cat#Z0334), and rabbit polyclonal anti-Iba-1 (1:200, FUJIFILM Wako). Secondary antibodies for visualization were rabbit anti-chicken IgY (1:500, Texas Red, Abcam, Cat#ab6751) for MBP and goat anti-rabbit IgG (1:1000, Alexa Fluor® 488, ThermoFisher, A11008) for GFAP and Iba-1.

In each group, the MBP fluorescence intensity in corpus callosum was corrected for background signal. Three slides per animal were analyzed, and the corrected values were averaged. These averages were then normalized to the mean fluorescence intensity of the myelinated region in the intact group, which was considered 100%. Also, the number of marker-positive cells ($GFAP^+$, Iba-1^+) was counted and divided by the total number of DAPI-stained nuclei, yielding the percentage of marker-positive cells per section. These values were then averaged within each group.

2.5. Statistical analysis

Data analysis was conducted blindly using GraphPad Prism v.9.0.0. First, the normality of data distribution was assessed. Statistical graphs represent at least three experiments, with each data point corresponding to a biological replicate or sections in an individual animal. One-way ANOVA with Tukey's test was applied to the antioxidant test, cell viability, and histological analysis data. The results are reported as mean ± SEM, with p-values < 0.001 considered statistically significant.

3 Results

3.1. Synthesis and characterization of CurP-CDs

CurP-CDs were synthesized hydrothermally, yielding a yellowish solution emitting blue fluorescence. CurP-CDs display a characteristic absorption peak between 250–280 nm, attributed to $\pi \rightarrow \pi^*$ electronic transitions of aromatic rings, sp^2 hybridized domains, and C=C double bonds. A shoulder at 300–320 nm corresponds to $n \rightarrow \pi^*$ transitions associated with surface C=O groups.[38] As shown in Fig. 1b, CurP-CDs exhibit excitation-dependent photoluminescence, with red-shifted emission and intensity changes observed from 370 to 420 nm excitation. The maximum fluorescence intensity observed at 488 nm following 390 nm excitation suggests that the substance contains a conjugated core structure, such as aromatic rings or polycyclic aromatic hydrocarbons, which lowers the energy gap and leads to a significant stokes shift. Smaller sp^2 domains in the core contribute to higher energy blue emission, while functional groups (*e.g.*, –OH, and $–NH_2$) may modify the fluorescence intensity and wavelength through electron donation or inductive effects[39] (Fig. 1a and b). FTIR analysis was performed to investigate the composition and functional groups. Peaks at 3274 cm^{-1} and 1599 cm^{-1} correspond to N–H stretching and bending vibrations, respectively. O–H stretching vibrations appear in the 3200–3500 cm^{-1} range, with bending vibrations at 1360 cm^{-1}. C–H stretching vibrations are observed at 2930 cm^{-1}, with bending vibrations at 1452 cm^{-1} and 750 cm^{-1}. Carboxylic acid (COOH) stretching vibrations are identified at 1701 cm^{-1}. Carbonyl (C=O) groups show bending vibrations at 817 cm^{-1} and 699 cm^{-1}. Peaks at 1268 cm^{-1}, 1122 cm^{-1}, and 1029 cm^{-1} indicate C–O and C–N stretching, while a peak at 1513 cm^{-1} corresponds to nitro (N–O) vibrations. Due to the nature of the hydrothermal carbonization process, the molecular structures of the precursors undergo chemical transformation and reorganization. These findings confirm the incorporation of functional groups from precursors such as urea, citric acid, curcumin, and phenylalanine, reflecting the structural diversity of the carbon dots (Fig. 1c). TEM imaging revealed CurP-CDs as nanoparticles with a size distribution ranging from 3 to 6 nanometers with a mean diameter of 4.2 ±

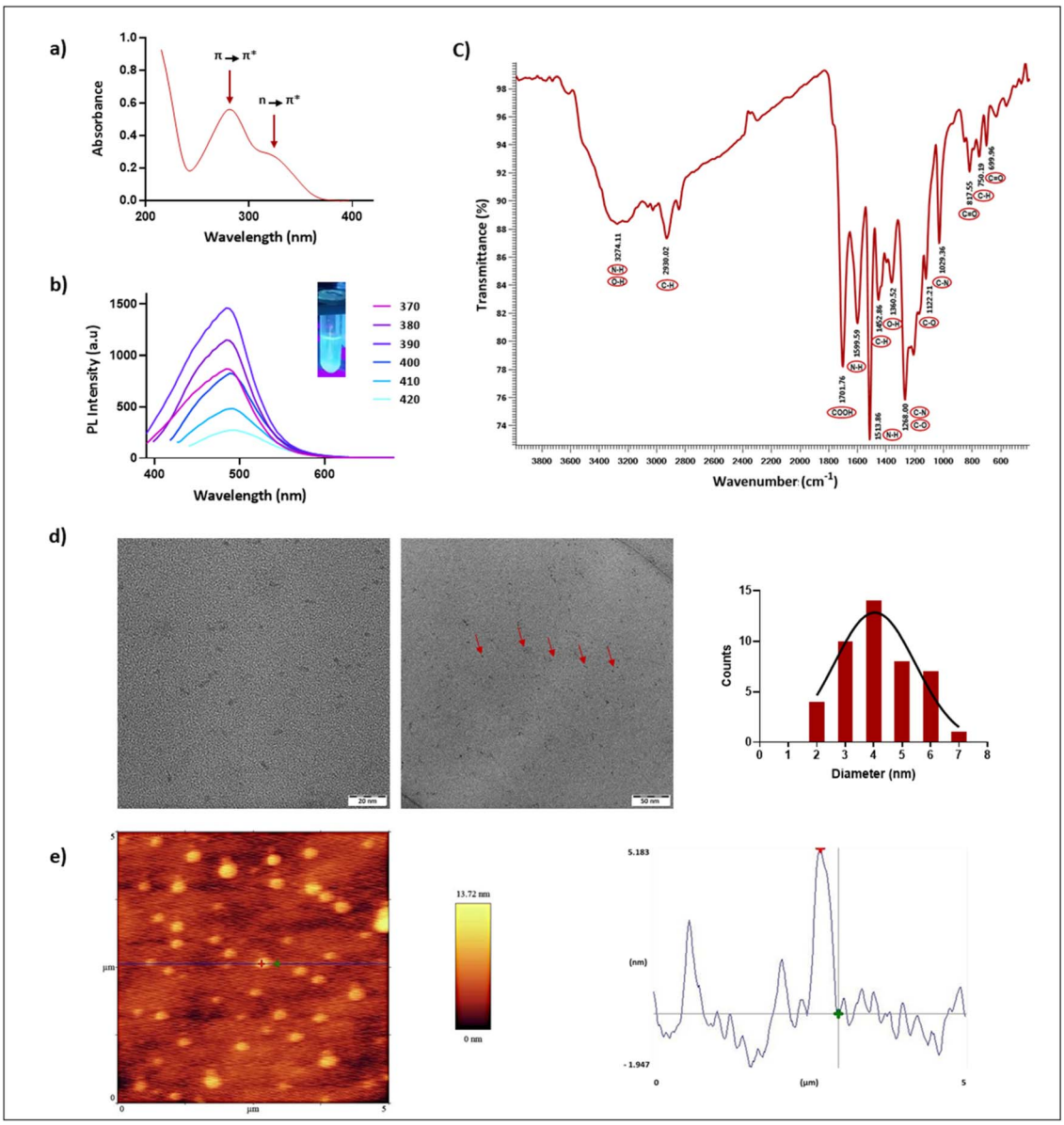

Fig. 1 Characterization of CurP-CDs. The optical properties of CurP-CDs showing (a) absorption peaks at 250–280 nm with a secondary shoulder at 300–320 nm and (b) emission at 488 nm upon excitation at 380 nm. (c) FTIR analysis of the carbon dots revealed key functional groups, including N–H, O–H, C–H, COOH, and C=O, indicating the presence of hydroxyl, amine, and carboxyl groups. (d) TEM imaging (scale bars of 20 nm (left) and 50 nm (right)) revealed that CurP-CDs are uniform and spherical, with particle sizes predominantly ranging from 3 to 6 nanometers with an average size of 4 nm. Statistical analysis and Gaussian fitting of the size distribution further confirmed the uniformity of the carbon dots. (e) AFM image of the CurP-CDs. The height profiles indicate a surface elevation of 5.1 nm for a typical CurP-CD.

0.8 nm (Fig. 1d). The AFM imaging demonstrated nanosized particles with heights ranging from 4 to 9 nm (Fig. 1e).

3.2. Antioxidation and cytocompatibility of CurP-CDs

Since the nature of the precursors plays a crucial role in determining the properties of the final product, it was expected that the synthesis of carbon dots from antioxidant-rich materials such as curcumin and citric acid would yield nanoparticles with antioxidant properties. The DPPH assay was conducted on various concentrations of carbon dots and ascorbic acid as a positive control. As shown in Fig. 2a, the carbon dots exhibit dose-dependent antioxidant activity. The MTT assay was performed to assess the cytocompatibility of varying concentrations of CurP-CDs on the U-87 MG cells in two different setups: incubation in complete culture medium and in serum-free medium with FBS added after 4 hours, followed by continuation in complete culture medium.

MTT assay results after 24 hours of incubation showed cell viability above 85%, with no significant difference compared to control groups that did not receive carbon dots. This confirms that the carbon dots are not toxic to the cells (Fig. 2b and c).

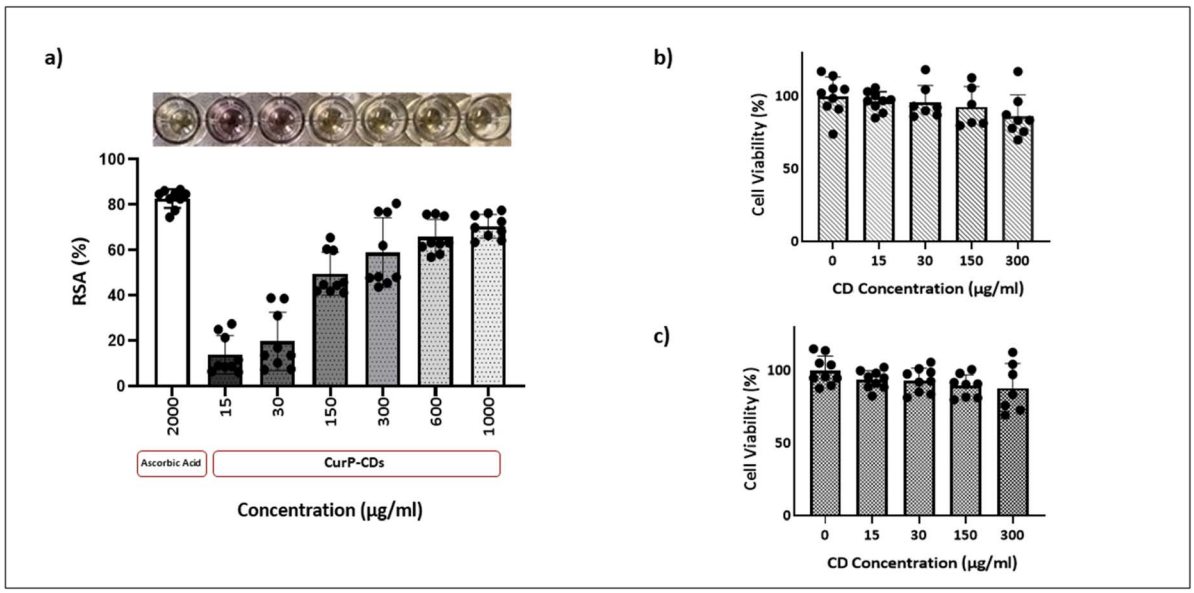

Fig. 2 Antioxidant activity and biological effects of CurP-CDs. (a) CurP-CDs' antioxidant activity was evaluated *via* the DPPH assay by measuring absorbance at 517 nm after reacting with various concentrations of CurP-CDs. At ≥ 300 µg ml^{-1}, comparable activity to ascorbic acid (positive control), with no statistically significant difference ($p > 0.001$), was observed. (b) The MTT assay was performed to assess the cytotoxicity of CurP-CDs (0–300 µg ml^{-1}) on U-87 MG cells for 24 hours, while FBS exists throughout the experiment or (c) added 4 hours post-treatment with CurP-CDs. Statistical analysis indicated no significant differences between the treated and control groups ($p > 0.001$), confirming the biocompatibility of the nanoparticles.

3.3. CurP-CDs reduced demyelination

The effects of CurP-CDs on myelin damage were evaluated using FluoroMyelin, Luxol fast blue, and MBP staining. FluoroMyelin and MBP immunofluorescence staining on cryo-sections showed higher myelin intensity and content in LPC + CurP-CDs treated groups compared to the LPC + PBS group, though lower than intact groups. Both FluoroMyelin and MBP analyses revealed a significant increase on day 3 post-injury, but not on day 7 (Fig. 3a, b, d and e). Similarly, LFB staining indicated lower extent of demyelinated areas in LPC + CurP-CD groups on days 3 and 7 compared to the LPC + PBS group (Fig. 3c and f). Overall, the assessment of fluorescence signal intensity as an indicator of myelin content, along with the examination of demyelinated areas in tissue sections, suggests reduced damage in the groups treated with CurP-CDs. This effect is most pronounced on the third day post-treatment, corresponding to the peak of inflammation in the LPC-induced model. These findings collectively support the protective effects of CurP-CDs on myelin integrity.

3.4. CurP-CDs reduced astroglial and microglial activation

As mentioned before, astrocytes and microglia are involved in the inflammatory process of MS. LPC injection induces astrogliosis, initially aimed at preventing damage, but prolonged activation impedes myelin repair.[40] To evaluate the impact of CurP-CDs on CNS endogenous inflammatory cells and gliosis, immunohistochemical staining for GFAP (astrogliosis) and Iba-1 (microgliosis) was performed. GFAP staining revealed active astrocytes, with an increase in their numbers on day 3 post-injury, which gradually decreased by day 7. In the CurP-CD-treated groups, the number of GFAP+ cells significantly decreased on day 3 compared to the model group. On day 7, carbon dot-treated mice exhibited a decreasing trend in GFAP+ cells, though it was not statistically significant (Fig. 4a and c). Furthermore, microglia as rare glial cells under physiological conditions were assessed by Iba-1 staining. The results showed increased microglia on day 3, with a decrease by day 7 in model groups. CurP-CD treatment significantly reduced microglia at both time points (Fig. 4b and d). Overall, CurP-CDs demonstrated a significant effect on inflammation and inhibited the damage extension.

4 Discussion

Considering inflammation as a major driver of MS progression, making anti-inflammatory and immune-modulating drugs is essential for the treatment. However, long-term use of these medications can harm vital organs, underscoring the need for safer therapeutic options.[41] On the other hand, activated glial cells, such as astrocytes and microglia, form glial scars and release inflammatory factors that damage myelin and axons in MS patients. Consequently, inhibiting gliosis is pivotal for promoting myelin repair in the CNS.[28]

Polyphenols inhibit cyclooxygenase and lipoxygenase, reducing inflammation by blocking cytokines such as TNF-α, IL-1, IL-6, and IFN-γ.[42] Curcumin, a polyphenolic compound, possesses neuroprotection in animal models, but its hydrophobic nature and the BBB limit its *in vivo* effectiveness. Carbon dots derived from curcumin offer a promising solution.[17]

In this study, CurP-CDs were synthesized *via* a one-pot hydrothermal method using curcumin, citric acid,

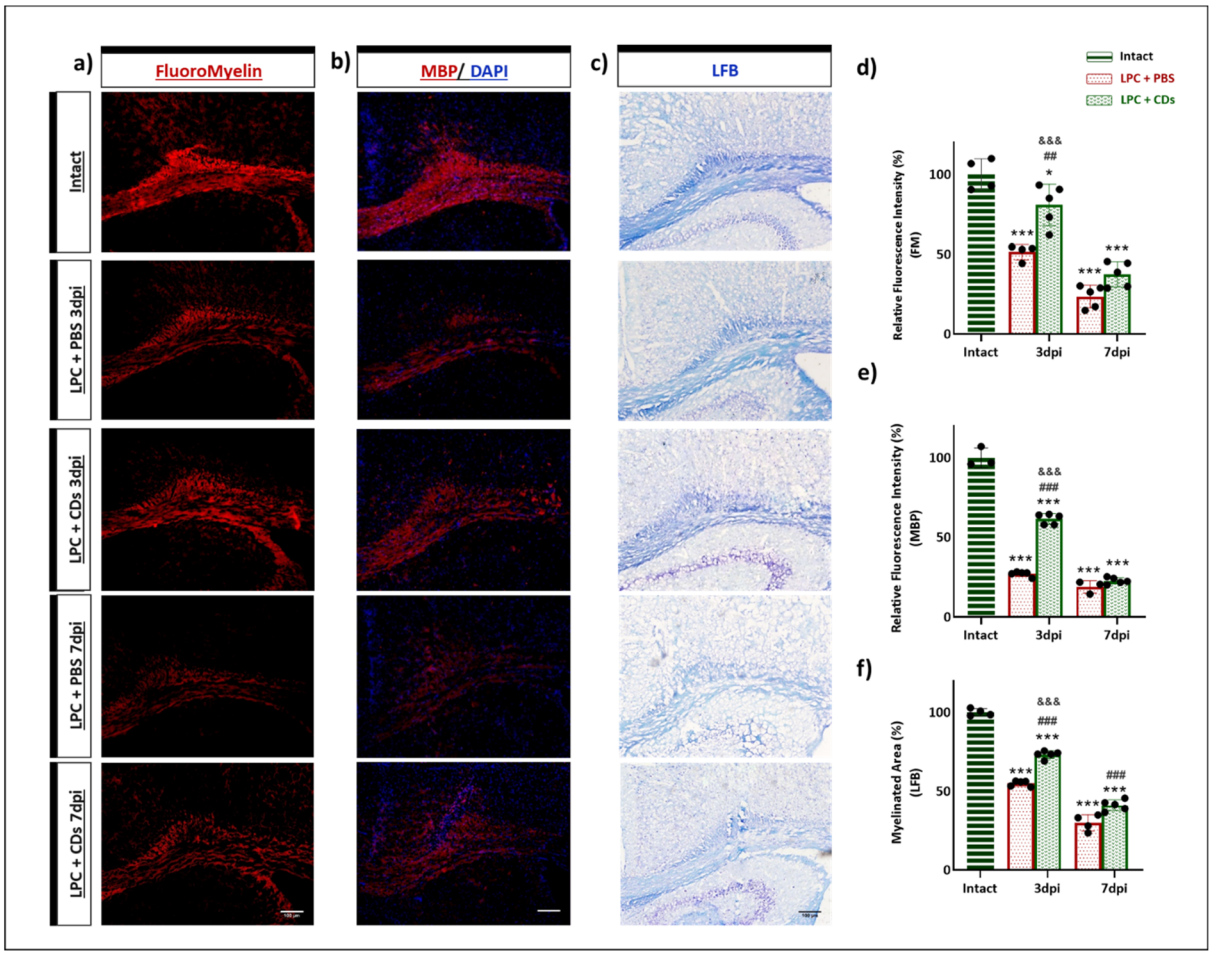

Fig. 3 Protective effects of CurP-CDs on myelin integrity post-injury. Figures represent (a) FluoroMyelin staining, (b) MBP immunofluorescence staining and (c) LFB staining at the LPC injection site in different experimental groups, and (d, e and f) quantitative analysis to assess myelination levels at lesion sites. All relative fluorescence values are normalized to the intact control group, which is set at 100%. Statistical significance is indicated by symbols: (*) *vs.* Intact, (#) *vs.* LPC + PBS, and (&) LPC + CDs 7 dpi. *vs.* LPC + CDs 3 dpi. Single, double, and triple symbols correspond to $p < 0.05$, $p < 0.01$, and $p < 0.001$, respectively. Data represent $n = 4–5$ per group, analyzed using one-way ANOVA followed by Tukey's post-hoc test. All images are shown at the same scale; scale bar: 100 μm.

phenylalanine, and urea. Each precursor functions as a specific component in the synthesis: curcumin served as a natural antioxidant-rich carbon source; citric acid contributed to stability and carbon framework formation;[18] phenylalanine as a nitrogen source and functionalizing agent; and urea as an additional nitrogen donor to enhance surface passivation and fluorescence properties.[18]

During carbon dot synthesis, precursors decompose and reorganize into nanostructures. Thus, precursor structures aren't fully preserved.[17] Incomplete carbonization may result in the partial retention of molecular structures on the nanoparticle surface.[38] Phenylalanine, which is the precursor of tyrosine, which itself is the precursor to catecholamines, naturally binds to relevant transporters on the blood–brain barrier (BBB).[43] Phenylalanine as a component used in the preparation of CurP-CDs may allow interactions with BBB transporters. However, this cannot be stated with certainty and requires further experimental validation. Herein, the nanoparticles were administered *via* intracerebellar injection, thereby bypassing the need to cross the BBB. Also, we anticipated the presence of functional groups associated with radical scavenging processes, such as hydroxyl groups (–OH), which donate hydrogen atoms, a common mechanism in natural antioxidants; carboxyl groups (–COOH), which donate electrons; and carbonyl groups (C=O), which contribute through electron transfer and hydrogen atom donation (as seen in flavonoids). This hypothesis was confirmed through FTIR analysis, which validated the presence of these functional groups. These findings were promising, suggesting potential anti-inflammatory effects of CDs in an animal model. Amine groups enhance solubility, drug absorption, and targeted delivery through biological membranes. Molecules, upon ionization to form ammonium ions (NH_3^+), are capable of efficiently traversing biological membranes *via* specific transport mechanisms.[44] The charge of carbon dots plays a crucial role in their biological function. As shown in Fig. 1S, CurP-CDs have a negative zeta potential (approximately −20 mV), which mainly originates from the deprotonation of –COOH groups. This is supported by FTIR analysis, which confirmed the presence of functional groups such as –COOH, –OH, C=O, and C–O on the nanoparticle surface. Negatively charged carbon dots are more

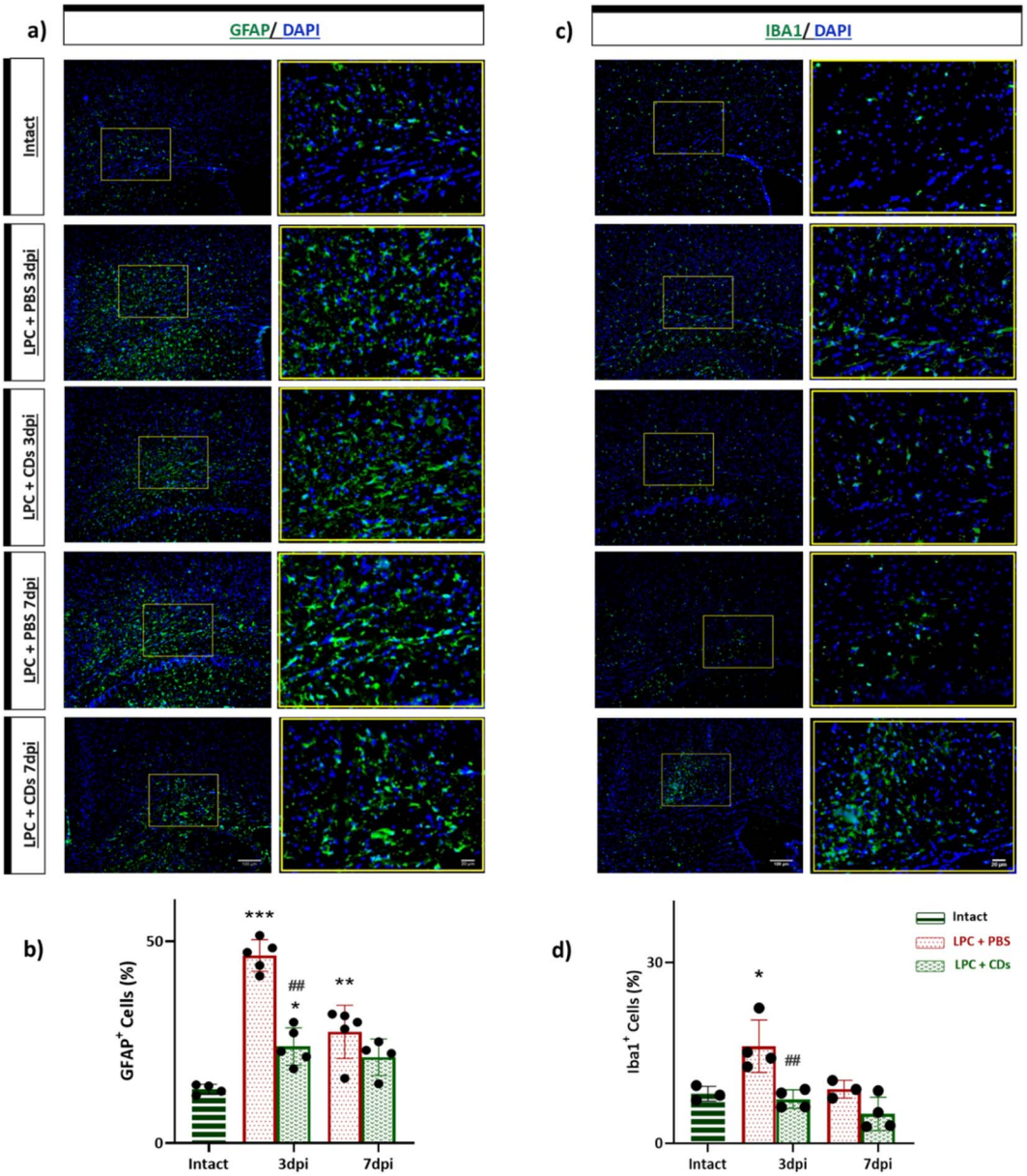

Fig. 4 CurP-CDs decreased astrogliosis in a myelin damage model. Figures represent (a and c) immunofluorescence staining against GFAP and Iba-1 as specific markers of astrocyte and microglia respectively. (b and d) Quantitative analysis to assess number of cells associated with inflammation. The percentage of positive cells was calculated relative to total DAPI stained nuclei and averaged per group. Statistical significance is indicated by symbols: (*) *vs.* Intact, and (#) *vs.* LPC + PBS. Single, double, and triple symbols correspond to $p < 0.05$, $p < 0.01$, and $p < 0.001$, respectively. Data represent $n = 3$–5 per group, analyzed using one-way ANOVA followed by Tukey's post-hoc test. All images are shown at the same scale; scale bar: 100 μm.

biocompatible and stable in aqueous environments due to electrostatic repulsion between similarly charged particles. On the other hand, positively charged carbon dots facilitate endocytosis by interacting with negatively charged membrane proteoglycans but are prone to binding with nucleic acids and proteins, increasing the likelihood of opsonization and reduced renal filtration, leading to greater body retention.[45] Hydrophilic molecules are able to diffuse in the interstitial fluid and move through the cerebrospinal fluid in the CNS.[18]

Astrocytes are vital mediators of growth, function, homeostasis, and brain plasticity. They also help in scavenging free radicals. In several neurodegenerative diseases, the elevated expression of glial fibrillary acidic protein (GFAP), vimentin, and nestin triggers astrocyte activation or astrogliosis. Once activated, they lose their regulatory function and initiate inflammatory responses, leading to neuronal death.[46] Microglia and macrophages in damaged regions with demyelination strongly express NADPH oxidase, indicating oxidative tissue damage.[10] Our findings demonstrate that CurP-CDs effectively

reduced number of astrocytes and microglia as the key drivers of inflammation and attenuate glial activation in the lysolecithin-induced model of MS. Additionally, histological analyses revealed significantly higher myelin preservation in CurP-CD-treated animals compared to controls, as shown by increased FluoroMyelin and MBP staining and reduced demyelinated areas in LFB-stained sections, indicating the ability of CDs to prevent inflammatory damage within the corpus callosum. The effects of CurP-CDs were significant on day 3 post-injection, a time point associated with the inflammation peak in this model. The reduced effects on myelin protection and astrogliosis on day 7 reflect the short-term effect of CurP-CDs. Further pharmacokinetic and biodistribution investigations are required to optimize the dosing regimen and treatment time course. One supporting piece of evidence is a study conducted by M. Naeimi *et al.*, in which enhancing curcumin solubility by loading it into chitosan–alginate–sodium tripolyphosphate nanoparticles significantly reduced demyelinated areas, glial activation, and inflammation in the LPC mice model. The protective effects on myelination are attributed to anti-inflammatory actions, glial inhibition, and reduced oxidative stress.[28]

5 Conclusion

Overall, this study demonstrates that curcumin-derived carbon dots (CurP-CDs) hold potential as a therapeutic option for MS, particularly during inflammatory phases. CurP-CDs exhibited neuroprotective effects by reducing myelin damage, preserving myelin integrity, and attenuating astrogliosis and microgliosis in an LPC-induced MS model; these effects were most notable on day 3 post-injection. These outcomes are likely linked to the antioxidant and anti-inflammatory functional groups present on the nanoparticle surface. Although the results are encouraging, further studies are needed to clarify the underlying mechanisms, determine optimal dosing, and assess the long-term safety and effectiveness of CurP-CDs.

Ethics approval and consent to participate

Animal experimentation was approved by the institutional ethics committee, approval number IR.MODARES.AEC.1402.004.

Author contributions

Ladan DaeiRezaei: writing – original draft, investigation, methodology, visualization, conceptualization. Maryam Nikkhah & Mohammad Javan: conceptualization, project administration, supervision, resources, validation, writing – review & editing. Elham Parand Avar: investigation, methodology.

Conflicts of interest

Authors declare no conflicts of interest.

Abbreviations

MS	Multiple sclerosis
LPC	Lysophosphatidylcholine
CDs	Carbon dots
CNS	Central nervous system
RRMS	Relapse-remitting multiple sclerosis
BBB	Blood–brain barrier
RT	Room temperature
DLS	Dynamic light scattering
TEM	Transmission electron microscopy
UV-vis	Ultraviolet-visible
PBS	Phosphate-buffered saline
Dpi	Days post-LPC injection
PFA	Paraformaldehyde
FM	FluoroMyelin
LFB	Luxol fast blue
Iba-1	Ionized calcium-binding adapter molecule 1
GFAP	Glial fibrillary acidic protein
MBP	Myelin basic protein

Data availability

All the generated and analyzed data are included in this published version. Additional details are available *via* reasonable inquiry to the corresponding author.

Supplementary information (SI) is available. See DOI: https://doi.org/10.1039/d5na00261c.

Acknowledgements

This study was partially supported by the Research Council of Tarbiat Modares University.

References

1 O. H. Kantarci, Phases and phenotypes of multiple sclerosis, *Continuum*, 2019, **25**(3), 636–654.
2 R. P. Moura, *et al.*, Functionalized retinoic acid lipid nanocapsules promotes a two-front attack on inflammation and lack of demyelination on neurodegenerative disorders, *J. Controlled Release*, 2023, **358**, 43–58.
3 A. Rayatpour, *et al.*, Ferroptosis inhibition by deferiprone, attenuates myelin damage and promotes neuroprotection in demyelinated optic nerve, *Sci. Rep.*, 2022, **12**(1), 19630.
4 K. Borziak and J. Finkelstein, X-linked genetic risk factors that promote autoimmunity and dampen remyelination are associated with multiple sclerosis susceptibility, *Mult. Scler. Relat. Disord.*, 2022, **66**, 104065.
5 J. A. Hollenbach and J. R. Oksenberg, The immunogenetics of multiple sclerosis: A comprehensive review, *J. Autoimmun.*, 2015, **64**, 13–25.
6 M. Chountoulesi and C. Demetzos, Promising nanotechnology approaches in treatment of autoimmune diseases of central nervous system, *Brain Sciences*, 2020, **10**(6), 338.

7 S. Haase and R. A. Linker, Inflammation in multiple sclerosis, *Ther. Adv. Neurol. Disord.*, 2021, **14**, 17562864211007687.
8 L. Zare, *et al.*, Targeted drug delivery into glial scar using CAQK peptide in a mouse model of multiple sclerosis, *Brain Commun.*, 2023, **5**(6), fcad325.
9 S. Dedoni, *et al.*, An overall view of the most common experimental models for multiple sclerosis, *Neurobiol. Dis.*, 2023, 106230.
10 H. Lassmann, Multiple sclerosis pathology, *Cold Spring Harbor Perspect. Med.*, 2018, **8**(3), a028936.
11 S. Waxman, J. Kocsis and K. Nitta, Lysophosphatidyl choline-induced focal demyelination in the rabbit corpus callosum: Light-microscopic observations, *J. Neurol. Sci.*, 1979, **44**(1), 45–53.
12 S. Farhangi, *et al.*, Peptide mediated targeted delivery of gold nanoparticles into the demyelination site ameliorates myelin impairment and gliosis, *Nanomed. Nanotechnol. Biol. Med.*, 2023, **47**, 102609.
13 E. Eitan, *et al.*, Combination therapy with lenalidomide and nanoceria ameliorates CNS autoimmunity, *Exp. Neurol.*, 2015, **273**, 151–160.
14 X.-X. Fu, *et al.*, Novel nano-carriers with N-formylmethionyl-leucyl-phenylalanine-modified liposomes improve effects of C16-angiopoietin 1 in acute animal model of multiple sclerosis, *Drug Delivery*, 2023, **30**(1), 2241664.
15 N. Rahiman, *et al.*, Recent advancements in nanoparticle-mediated approaches for restoration of multiple sclerosis, *J. Controlled Release*, 2022, **343**, 620–644.
16 A. E. H. Youssef, *et al.*, LINGO-1 siRNA nanoparticles promote central remyelination in ethidium bromide-induced demyelination in rats, *J. Physiol. Biochem.*, 2019, **75**, 89–99.
17 Q. Zeng, *et al.*, Precursor-dependent structural diversity in luminescent carbonized polymer dots (CPDs): the nomenclature, *Light: Sci. Appl.*, 2021, **10**(1), 142.
18 W. Zhang, *et al.*, Carbon dots: A future Blood–Brain Barrier penetrating nanomedicine and drug nanocarrier, *Int. J. Nanomed.*, 2021, 5003–5016.
19 Y. Zhou, *et al.*, Direct conjugation of distinct carbon dots as Lego-like building blocks for the assembly of versatile drug nanocarriers, *J. Colloid Interface Sci.*, 2020, **576**, 412–425.
20 A. Sharma, H.-K. Choi and H.-J. Lee, Carbon dots for the treatment of inflammatory diseases: An appraisal of in vitro and in vivo studies, *Oxid. Med. Cell. Longevity*, 2023, **2023**(1), 3076119.
21 X. Xu, *et al.*, Aspirin-based carbon dots, a good biocompatibility of material applied for bioimaging and anti-inflammation, *ACS Appl. Mater. Interfaces*, 2016, **8**(48), 32706–32716.
22 Y. Zhang, *et al.*, The neuroprotective effect of pretreatment with carbon dots from Crinis Carbonisatus (carbonized human hair) against cerebral ischemia reperfusion injury, *J. Nanobiotechnol.*, 2021, **19**(1), 257.
23 K. S. Jaiswal, *et al.*, Genistein carbon dots exhibit antioxidant and anti-inflammatory effects in vitro, *Colloids Surf., B*, 2023, **223**, 113173.
24 C. Dong, *et al.*, Carbon dots nanozyme for anti-inflammatory therapy via scavenging intracellular reactive oxygen species, *Front. Bioeng. Biotechnol.*, 2022, **10**, 943399.
25 Z. Qu, *et al.*, Synthesis of bifunctional carbon quantum dots for bioimaging and anti-inflammation, *Nanotechnology*, 2020, **31**(17), 175102.
26 B. C. Demirdöğen, Theranostic potential of graphene quantum dots for multiple sclerosis, *Mult. Scler. Relat. Disord.*, 2022, **68**, 104232.
27 J. Tosic, *et al.*, Graphene quantum dots inhibit T cell-mediated neuroinflammation in rats, *Neuropharmacology*, 2019, **146**, 95–108.
28 R. Naeimi, *et al.*, Curcumin-loaded nanoparticles ameliorate glial activation and improve myelin repair in lyolecithin-induced focal demyelination model of rat corpus callosum, *Neurosci. Lett.*, 2018, **674**, 1–10.
29 P. Bharmoria, *et al.*, Protein-olive oil-in-water nanoemulsions as encapsulation materials for curcumin acting as anticancer agent towards MDA-MB-231 cells, *Sci. Rep.*, 2021, **11**(1), 9099.
30 B. Barzegarzadeh, *et al.*, Conjugated linoleic acid-curcumin attenuates cognitive deficits and oxidative stress parameters in the ethidium bromide–induced model of demyelination, *Neurotoxic. Res.*, 2021, **39**, 815–825.
31 M. Mohajeri, *et al.*, Polymerized nano-curcumin attenuates neurological symptoms in EAE model of multiple sclerosis through down regulation of inflammatory and oxidative processes and enhancing neuroprotection and myelin repair, *Neuropharmacology*, 2015, **99**, 156–167.
32 M. Motavaf, *et al.*, Dendrosomal nanocurcumin promotes remyelination through induction of oligodendrogenesis in experimental demyelination animal model, *J. Tissue Eng. Regener. Med.*, 2020, **14**(10), 1449–1464.
33 M. Motavaf, *et al.*, Protective effects of a nano-formulation of curcumin against cuprizone-induced demyelination in the mouse corpus callosum, *Iran. J. Pharm. Res.*, 2020, **19**(3), 310.
34 Y. Kuang, *et al.*, A novel nanosystem realizing curcumin delivery based on Fe3O4@ carbon dots nanocomposite for Alzheimer's disease therapy, *Front. Bioeng. Biotechnol.*, 2020, **8**, 614906.
35 A. Fibriani, *et al.*, Curcumin-derived carbon-dots as a potential COVID-19 antiviral drug, *Heliyon*, 2023, **9**(9), e20089.
36 S. Rodríguez-Varillas, *et al.*, Biocompatibility and antioxidant capabilities of carbon dots obtained from tomato (Solanum lycopersicum), *Appl. Sci.*, 2022, **12**(2), 773.
37 C. Procaccini, *et al.*, Animal models of multiple sclerosis, *Eur. J. Pharmacol.*, 2015, **759**, 182–191.
38 K. J. Mintz, *et al.*, A deep investigation into the structure of carbon dots, *Carbon*, 2021, **173**, 433–447.
39 D. M. Jameson, *Introduction to Fluorescence*, Taylor & Francis, 2014.
40 T. R. Hammond, *et al.*, Astrocyte-derived endothelin-1 inhibits remyelination through notch activation, *Neuron*, 2014, **81**(3), 588–602.
41 J. A. French, *et al.*, Clinical studies and anti-inflammatory mechanisms of treatments, *Epilepsia*, 2017, **58**, 69–82.

42 K. B. Pandey and S. I. Rizvi, Plant polyphenols as dietary antioxidants in human health and disease, *Oxid. Med. Cell. Longev.*, 2009, **2**(5), 270–278.
43 J. D. Fernstrom and M. H. Fernstrom, Tyrosine, phenylalanine, and catecholamine synthesis and function in the brain2, *J. Nutr.*, 2007, **137**(6), 1539S–1547S.
44 L. L. Brunton and B. C. Knollmann, in *Goodman & Gilman's: the Pharmacological Basis of Therapeutics*, McGraw-Hill Education, New York, NY, 14th edn, 2023.
45 A. Truskewycz, *et al.*, Carbon dot therapeutic platforms: administration, distribution, metabolism, excretion, toxicity, and therapeutic potential, *Small*, 2022, **18**(16), 2106342.
46 S. Eghbaliferiz, *et al.*, Effects of curcumin on neurological diseases: focus on astrocytes, *Pharmacol. Rep.*, 2020, **72**(4), 769–782.